Active Damping of Rotating Positioning Platforms using Force Feedback

T. Dehaeze [1,3]**, C. Collette** [1,2]
[1] Precision Mechatronics Laboratory
University of Liege, Belgium

[2] BEAMS Department
Free University of Brussels, Belgium

[3] European Synchrotron Radiation Facility
Grenoble, France e-mail: **thomas.dehaeze@esrf.fr**

Abstract
Abstract text to be done

1   Introduction

Controller Poles are shown by black crosses (✖). Due to gyroscopic effects, the guaranteed robustness properties of Integral Force Feedback do not hold. Either the control architecture can be slightly modfied or mechanical changes in the system can be performed. This paper has been published The Matlab code that was use to obtain the results are available in [1].

2   Dynamics of Rotating Positioning Platforms

2.1   Model of a Rotating Positioning Platform

To study how the rotation of positioning platforms does affect the use of force feedback, a simple model is developed.

It represents an X-Y positioning stage on top of a Rotating Stage and is schematically represented in Figure 1.

Two frames of reference are used:

- $(\vec{i}_x, \vec{i}_y, \vec{i}_z)$ is an inertial frame
- $(\vec{i}_u, \vec{i}_v, \vec{i}_w)$ is a frame fixed on the Rotating Stage with its origin align with the rotation axis

The rotating stage is supposed to be ideal, meaning it is infinitely rigid and induces a rotation $\theta(t) = \Omega t$ where Ω is the rotational speed in $\mathrm{rad\,s^{-1}}$.

The parallel X-Y positioning stage consists of two orthogonal actuators represented by the three following elements in parallel:

- A spring with a stiffness k in $\mathrm{N\,m^{-1}}$
- A dashpot with a damping coefficient c in $\mathrm{N\,m^{-1}\,s}$

- An ideal force source F_u, F_v in N

The X-Y stage is supporting a payload with a payload with a mass m in kg. The position of the payload is represented by (d_u, d_v) expressed in the rotating frame $(\vec{i}_u, \vec{i}_v)$.
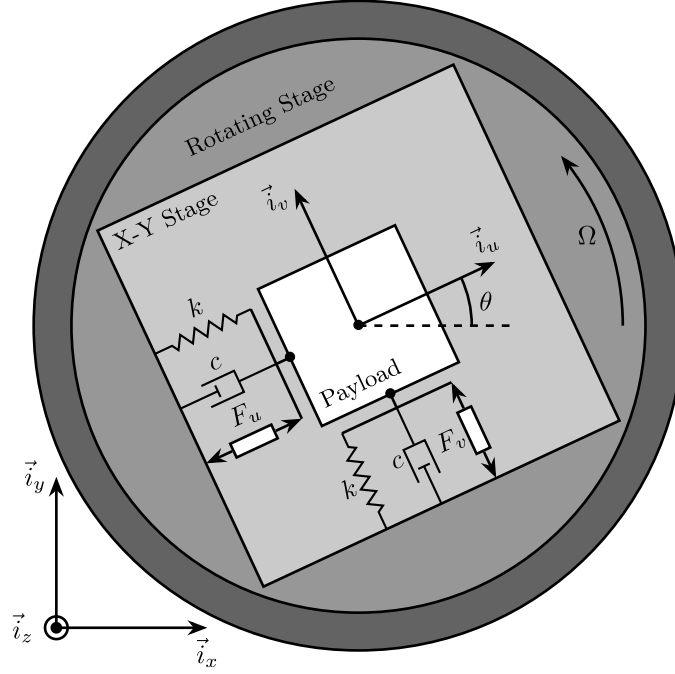

Figure 1: Schematic of the studied System

2.2 Equations of Motion

To obtain of equation of motion for the system represented in Figure 1, the Lagrangian equations are used:

$$\frac{d}{dt}\left(\frac{\partial L}{\partial \dot{q}_i}\right) + \frac{\partial D}{\partial \dot{q}_i} - \frac{\partial L}{\partial q_i} = Q_i \tag{1}$$

with $L = T - V$ is the Lagrangian, D is the dissipation function, and Q_i is the generalized force associated with the generalized variable $[q_1 \ q_2] = [d_u \ d_v]$:

$$T = \frac{1}{2}m\left(\left(\dot{d}_u - \Omega d_v\right)^2 + \left(\dot{d}_v + \Omega d_u\right)^2\right) \tag{2a}$$

$$V = \frac{1}{2}k\left(d_u{}^2 + d_v{}^2\right) \tag{2b}$$

$$D = \frac{1}{2}c\left(\dot{d}_u{}^2 + \dot{d}_v{}^2\right) \tag{2c}$$

$$Q_1 = F_u, \quad Q_2 = F_v \tag{2d}$$

Substituting equations (2) into (1) gives the two coupled differential equations:

$$m\ddot{d}_u + c\dot{d}_u + (k - m\Omega)d_u = F_u + 2m\Omega\dot{d}_v \tag{3a}$$

$$m\ddot{d}_v + c\dot{d}_v + (k \underbrace{- m\Omega}_{\text{Centrif.}})d_v = F_v \underbrace{- 2m\Omega\dot{d}_u}_{\text{Coriolis}} \tag{3b}$$

The rotation of the XY positioning platform induces two Gyroscopic effects:

- Coriolis Forces: that adds coupling between the two orthogonal controlled directions

- Centrifugal forces: that can been seen as negative stiffness

2.3 Transfer Functions in the Laplace domain

To study the dynamics of the system, the differential equations of motions (3) are transformed in the Laplace domain and the transfer functions from $[F_u,\ F_v]$ to $[d_u,\ d_v]$ are obtained:

$$\begin{bmatrix} d_u \\ d_v \end{bmatrix} = \boldsymbol{G}_d \begin{bmatrix} F_u \\ F_v \end{bmatrix} \tag{4}$$

with $\boldsymbol{G}_d$ a 2×2 transfer function matrix

$$\boldsymbol{G}_d = \begin{bmatrix} \dfrac{ms^2+cs+k-m\Omega^2}{(ms^2+cs+k-m\Omega^2)^2+(2m\Omega s)^2} & \dfrac{2m\Omega s}{(ms^2+cs+k-m\Omega^2)^2+(2m\Omega s)^2} \\ \dfrac{-2m\Omega s}{(ms^2+cs+k-m\Omega^2)^2+(2m\Omega s)^2} & \dfrac{ms^2+cs+k-m\Omega^2}{(ms^2+cs+k-m\Omega^2)^2+(2m\Omega s)^2} \end{bmatrix} \tag{5}$$

One can verify that without rotation ($\Omega = 0$) the system becomes equivalent as to two uncoupled one degree of freedom mass-spring-damper systems:

$$d_u = \frac{1}{ms^2 + cs + k} F_u \tag{6a}$$

$$d_v = \frac{1}{ms^2 + cs + k} F_v \tag{6b}$$

2.4 Change of Variables / Parameters for the study

In order to make this study less dependent on the system parameters, the following change of variable is performed:

- $\omega_0 = \sqrt{\dfrac{k}{m}}$: Natural frequency of the mass-spring system in $\mathrm{rad/s}$
- $\xi = \dfrac{c}{2\sqrt{km}}$: Damping ratio

The transfer function matrix (5) becomes equal to

$$\boldsymbol{G}_d = \frac{1}{k} \begin{bmatrix} \dfrac{\frac{s^2}{\omega_0^2}+2\xi\frac{s}{\omega_0}+1-\frac{\Omega^2}{\omega_0^2}}{\left(\frac{s^2}{\omega_0^2}+2\xi\frac{s}{\omega_0}+1-\frac{\Omega^2}{\omega_0^2}\right)^2+\left(2\frac{\Omega}{\omega_0}\frac{s}{\omega_0}\right)^2} & \dfrac{2\frac{\Omega}{\omega_0}\frac{s}{\omega_0}}{\left(\frac{s^2}{\omega_0^2}+2\xi\frac{s}{\omega_0}+1-\frac{\Omega^2}{\omega_0^2}\right)^2+\left(2\frac{\Omega}{\omega_0}\frac{s}{\omega_0}\right)^2} \\ \dfrac{-2\frac{\Omega}{\omega_0}\frac{s}{\omega_0}}{\left(\frac{s^2}{\omega_0^2}+2\xi\frac{s}{\omega_0}+1-\frac{\Omega^2}{\omega_0^2}\right)^2+\left(2\frac{\Omega}{\omega_0}\frac{s}{\omega_0}\right)^2} & \dfrac{\frac{s^2}{\omega_0^2}+2\xi\frac{s}{\omega_0}+1-\frac{\Omega^2}{\omega_0^2}}{\left(\frac{s^2}{\omega_0^2}+2\xi\frac{s}{\omega_0}+1-\frac{\Omega^2}{\omega_0^2}\right)^2+\left(2\frac{\Omega}{\omega_0}\frac{s}{\omega_0}\right)^2} \end{bmatrix} \tag{7}$$

During the rest of this study, the following parameters are used for numerical analysis

- $\omega_0 = 1\,\mathrm{rad\,s^{-1}}, \xi = 0.025 = 2.5\,\%$
- $k = 1\,\mathrm{N/m}, m = 1\,\mathrm{kg}, c = 0.05\,\mathrm{N\,m^{-1}\,s}$

2.5 System Dynamics and Campbell Diagram

The poles of $\boldsymbol{G}_d$ are the complex solutions p of

$$\left(\frac{p^2}{\omega_0^2} + 2\xi\frac{p}{\omega_0} + 1 - \frac{\Omega^2}{\omega_0^2}\right)^2 + \left(2\frac{\Omega}{\omega_0}\frac{p}{\omega_0}\right)^2 = 0 \tag{8}$$

Supposing small damping ($\xi \ll 1$), two pairs of complex conjugate poles are obtained:

$$p_+ = -\xi\omega_0 \left(1 + \frac{\Omega}{\omega_0}\right) \pm j\left(\omega_0 + \Omega\right) \tag{9a}$$

$$p_- = -\xi\omega_0 \left(1 - \frac{\Omega}{\omega_0}\right) \pm j\left(\omega_0 - \Omega\right) \tag{9b}$$

When the rotation speed in non-null, the resonance frequency is split into two pairs of complex conjugate poles. As the rotation speed increases, p_+ goes to higher frequencies and p_- to lower frequencies.

When the rotational speed Ω reaches ω_0, the real part p_- is positive meaning the system becomes unstable. The stiffness of the X-Y stage is too low to hold to rotating payload hence the instability. Stiff positioning platforms should be used if high rotational speeds or heavy payloads are used.

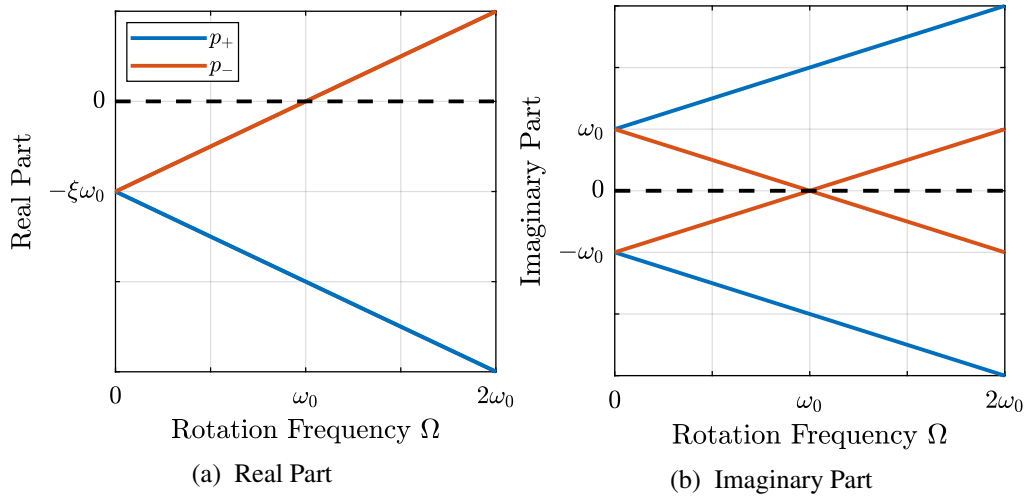This is graphically represented with the Campbell Diagram in Figure 2.

Figure 2: Campbell Diagram : Evolution of the complex and real parts of the system's poles as a function of the rotational speed Ω

Looking at the transfer function matrix $\boldsymbol{G}_d$ (7), one can see it has two distinct terms that can be studied separately:

- the direct (diagonal) terms
- the coupling (off-diagonal) terms

The bode plot of the direct and coupling terms are shown in Figure 3 for several rotational speed Ω.

Without rotation, the dynamics of the direct terms is equivalent to the dynamics of a one degree of freedom mass spring damper system and the coupling terms are null. As the rotational speed increases, the pair of complex conjugate poles is separated into two pairs of complex conjugate poles, one going to lower frequencies and the other to higher frequencies. When the

In the rest of this study, $\Omega < \omega_0$

3 Decentralized Integral Force Feedback

3.1 System Schematic and Control Architecture

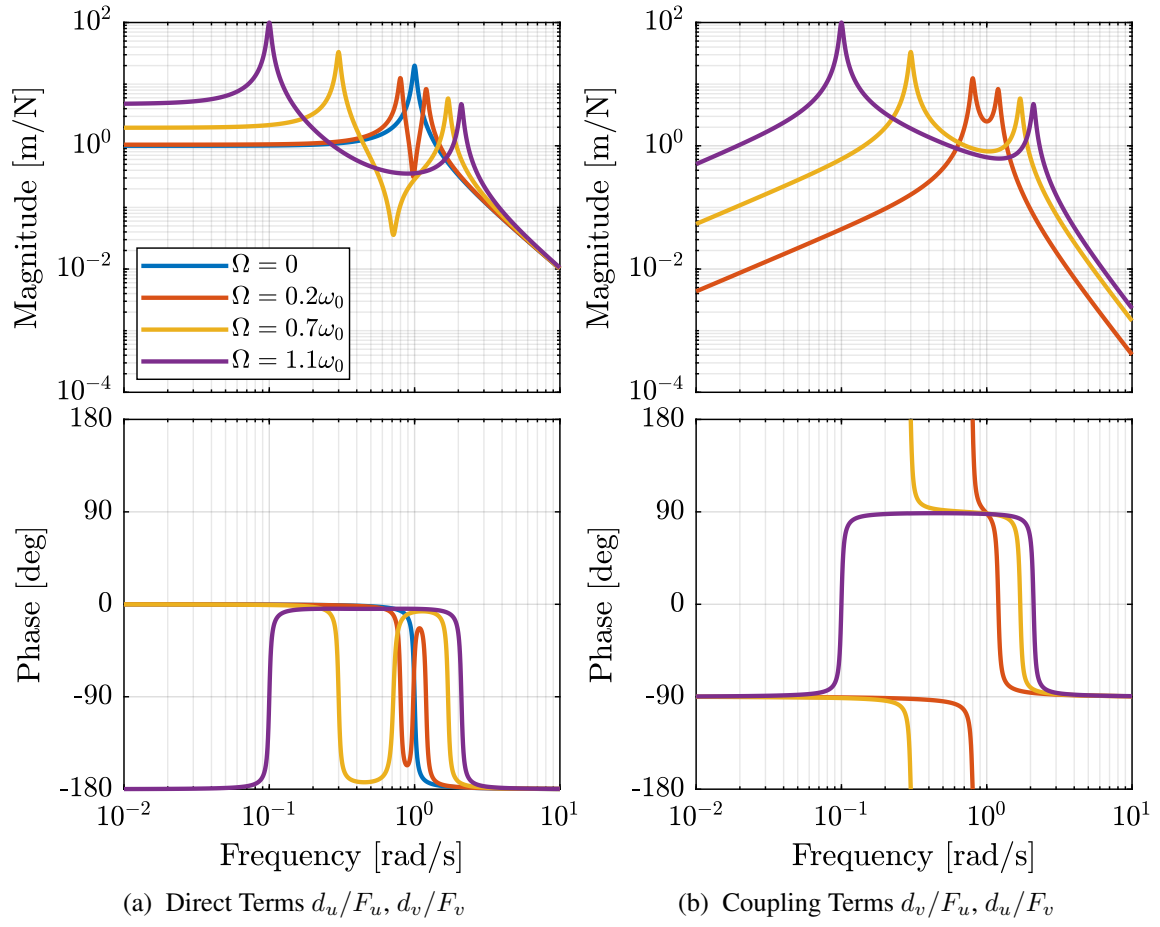Force Sensors are added in series with the actuators as shown in Figure 4.

(a) Direct Terms d_u/F_u, d_v/F_v

(b) Coupling Terms d_v/F_u, d_u/F_v

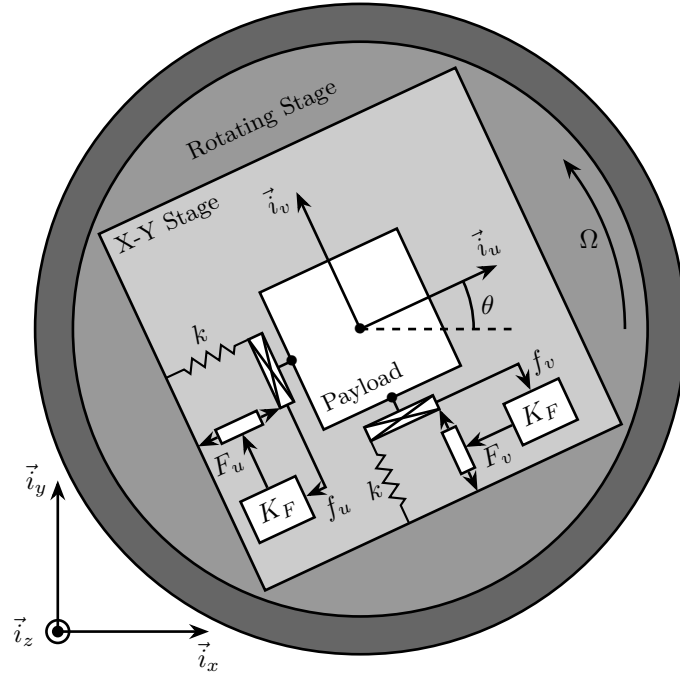Figure 3: Bode Plots for $\boldsymbol{G}_d$ for several rotational speed Ω

Figure 4: System with Force Sensors in Series with the Actuators. Decentralized Integral Force Feedback is used

3.2 Plant Dynamics

The forces measured by the force sensors are equal to:

$$\begin{bmatrix} f_u \\ f_v \end{bmatrix} = \begin{bmatrix} F_u \\ F_v \end{bmatrix} - (cs + k) \begin{bmatrix} d_u \\ d_v \end{bmatrix} \tag{10}$$

Re-injecting (7) into (10) yields:

$$\begin{bmatrix} f_u \\ f_v \end{bmatrix} = \boldsymbol{G}_f \begin{bmatrix} F_u \\ F_v \end{bmatrix} \tag{11}$$

with $\boldsymbol{G}_f$ a 2×2 transfer function matrix

$$\boldsymbol{G}_f = \begin{bmatrix} \dfrac{\left(\frac{s^2}{\omega_0{}^2}-\frac{\Omega^2}{\omega_0{}^2}\right)\left(\frac{s^2}{\omega_0{}^2}+2\xi\frac{s}{\omega_0}+1-\frac{\Omega^2}{\omega_0{}^2}\right)+\left(2\frac{\Omega}{\omega_0}\frac{s}{\omega_0}\right)^2}{\left(\frac{s^2}{\omega_0{}^2}+2\xi\frac{s}{\omega_0}+1-\frac{\Omega^2}{\omega_0{}^2}\right)^2+\left(2\frac{\Omega}{\omega_0}\frac{s}{\omega_0}\right)^2} & \dfrac{-\left(2\xi\frac{s}{\omega_0}+1\right)\left(2\frac{\Omega}{\omega_0}\frac{s}{\omega_0}\right)}{\left(\frac{s^2}{\omega_0{}^2}+2\xi\frac{s}{\omega_0}+1-\frac{\Omega^2}{\omega_0{}^2}\right)^2+\left(2\frac{\Omega}{\omega_0}\frac{s}{\omega_0}\right)^2} \\[3em] \dfrac{\left(2\xi\frac{s}{\omega_0}+1\right)\left(2\frac{\Omega}{\omega_0}\frac{s}{\omega_0}\right)}{\left(\frac{s^2}{\omega_0{}^2}+2\xi\frac{s}{\omega_0}+1-\frac{\Omega^2}{\omega_0{}^2}\right)^2+\left(2\frac{\Omega}{\omega_0}\frac{s}{\omega_0}\right)^2} & \dfrac{\left(\frac{s^2}{\omega_0{}^2}-\frac{\Omega^2}{\omega_0{}^2}\right)\left(\frac{s^2}{\omega_0{}^2}+2\xi\frac{s}{\omega_0}+1-\frac{\Omega^2}{\omega_0{}^2}\right)+\left(2\frac{\Omega}{\omega_0}\frac{s}{\omega_0}\right)^2}{\left(\frac{s^2}{\omega_0{}^2}+2\xi\frac{s}{\omega_0}+1-\frac{\Omega^2}{\omega_0{}^2}\right)^2+\left(2\frac{\Omega}{\omega_0}\frac{s}{\omega_0}\right)^2} \end{bmatrix} \tag{12}$$

The zeros of the diagonal terms of $\boldsymbol{G}_f$ are equal to (neglecting the damping)

$$z_c = \pm j\omega_0 \sqrt{\frac{1}{2}\sqrt{8\frac{\Omega^2}{\omega_0{}^2}+1}+\frac{\Omega^2}{\omega_0{}^2}+\frac{1}{2}} \tag{13a}$$

$$z_r = \pm \omega_0 \sqrt{\frac{1}{2}\sqrt{8\frac{\Omega^2}{\omega_0{}^2}+1}-\frac{\Omega^2}{\omega_0{}^2}-\frac{1}{2}} \tag{13b}$$

The frequency of the two complex conjugate zeros z_c (13a) is between the frequency of the two pairs of complex conjugate poles p_- and p_+ (9). This is the expected behavior of a collocated pair of actuator and sensor.

However, the two real zeros z_c induces an increase of +2 of the slope without change of phase (Figure 5). This represents non-minimum phase behavior.

The low frequency gain, for $\Omega < \omega_0$, is no longer zero:

$$\boldsymbol{G}_{f0} = \lim_{\omega \to 0} |\boldsymbol{G}_f(j\omega)| = \begin{bmatrix} \frac{-\Omega^2}{\omega_0{}^2-\Omega^2} & 0 \\ 0 & \frac{-\Omega^2}{\omega_0{}^2-\Omega^2} \end{bmatrix} \tag{14}$$

It increases with the rotational speed Ω.

3.3 Decentralized Integral Force Feedback

$$K_F(s) = g \cdot \frac{1}{s} \tag{15}$$

Also, as one zero has a positive real part, the **IFF control is no more unconditionally stable**. This is due to the fact that the zeros of the plant are the poles of the closed loop system with an infinite gain. Thus, for some finite IFF gain, one pole will have a positive real part and the system will be unstable.

At low frequency, the gain is very large and thus no force is transmitted between the payload and the rotating stage. This means that at low frequency, the system is decoupled (the force sensor removed) and thus the system is unstable.
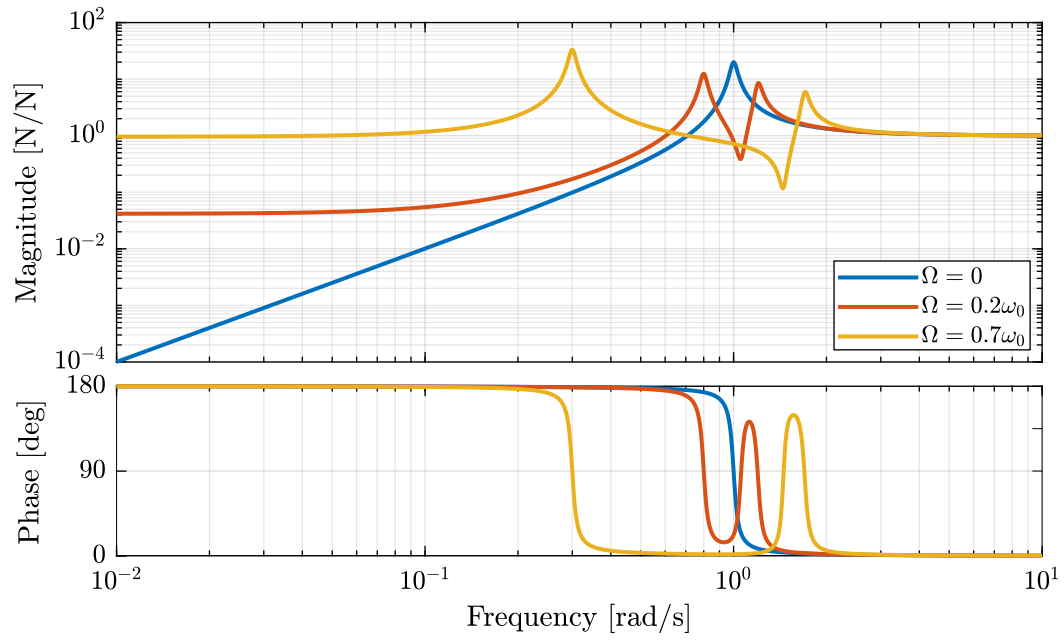
Figure 5: Bode plot of $\boldsymbol{G}_f$ for several rotational speeds Ω

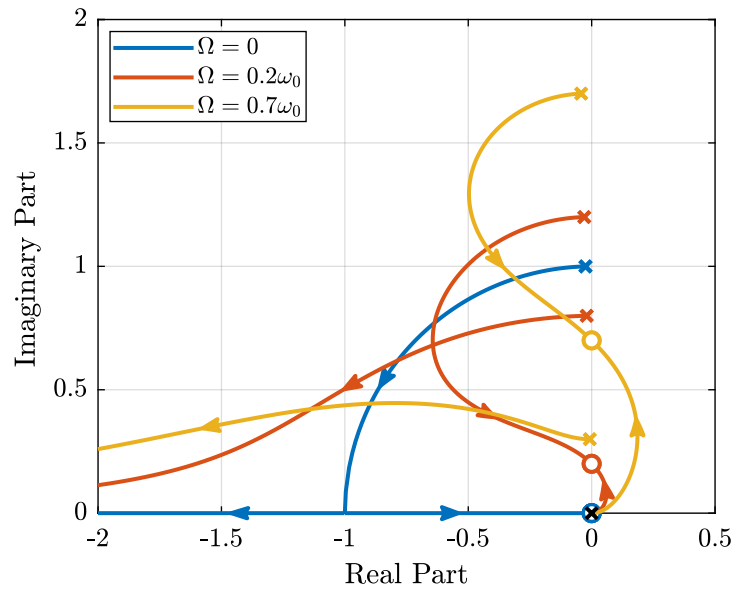
Figure 6: Root Locus for the Decentralized Integral Force Feedback

4 Integral Force Feedback with High Pass Filters

4.1 Modification of the Control Low

$$K_F(s) = g \cdot \frac{1}{s} \cdot \underbrace{\frac{s/\omega_i}{1 + s/\omega_i}}_{\text{HPF}} = g \cdot \frac{1}{s + \omega_i} \tag{16}$$
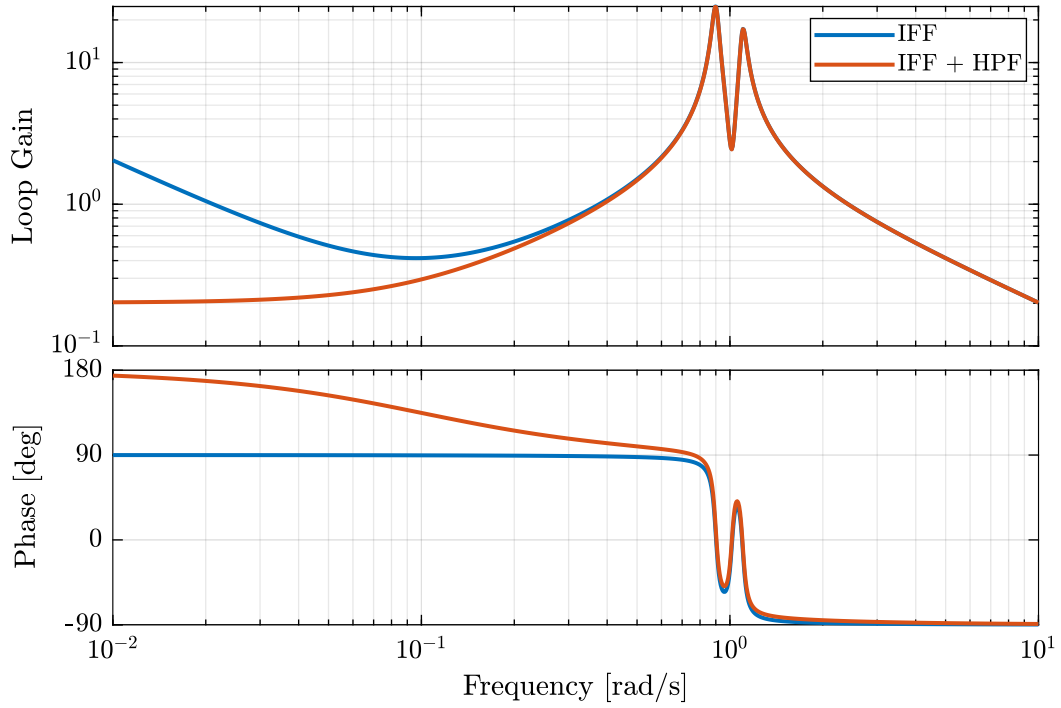
4.2 Feedback Analysis

Figure 7: Bode Plot of the Loop Gain for IFF with and without the HPF

$$g_{\text{max}} = \omega_i \left(\frac{{\omega_0}^2}{\Omega^2} - 1 \right) \tag{17}$$

4.3 Optimal Cut-Off Frequency

5 Integral Force Feedback with Parallel Springs

5.1 Stiffness in Parallel with the Force Sensor

5.2 Plant Dynamics

We define an adimensional parameter α, $0 \le \alpha < 1$, that describes the proportion of the stiffness in parallel with the actuator and force sensor:

$$k_p = \alpha k \tag{18a}$$
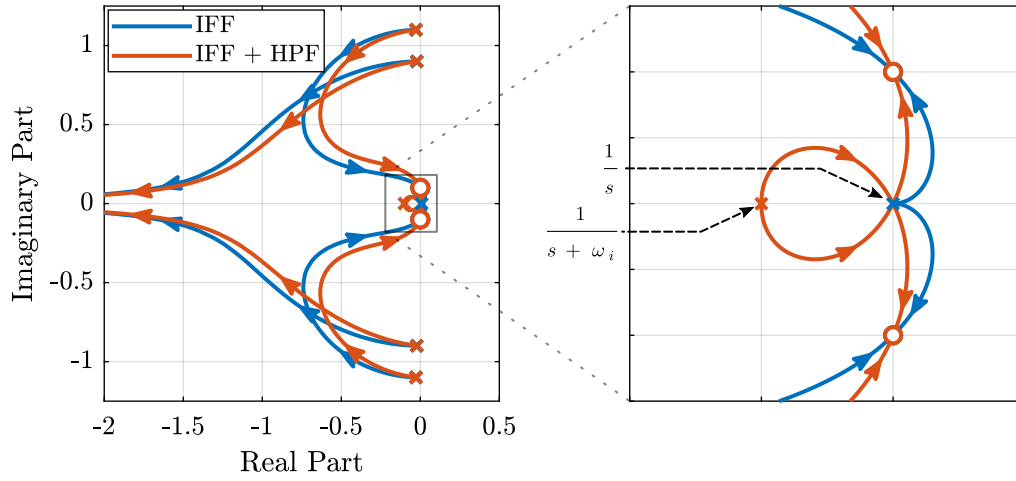$$k_a = (1 - \alpha)k \tag{18b}$$

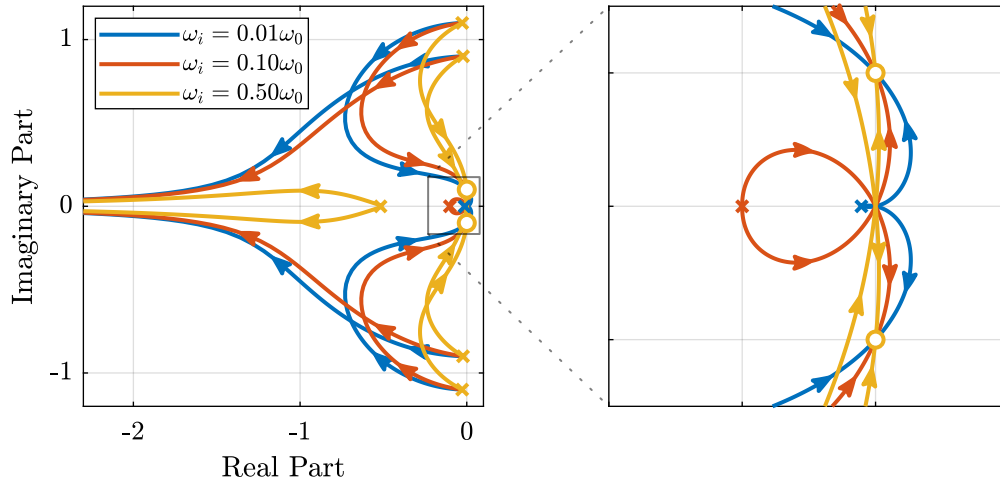Figure 8: Root Locus for IFF with and without the HPF

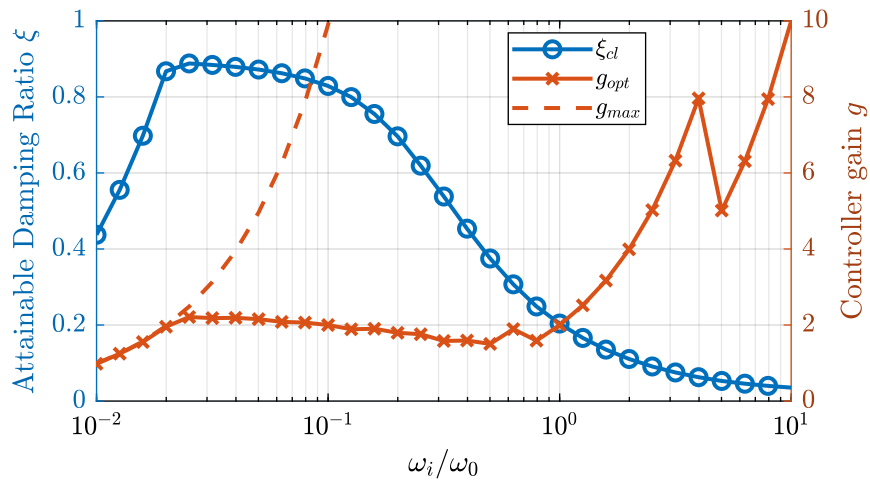Figure 9: Root Locus for several HPF cut-off frequencies ω_i

Figure 10: Attainable damping ratio ξ_{cl} as a function of the HPF cut-off frequency. Corresponding control gain g_{opt} and g_{max} are also shown
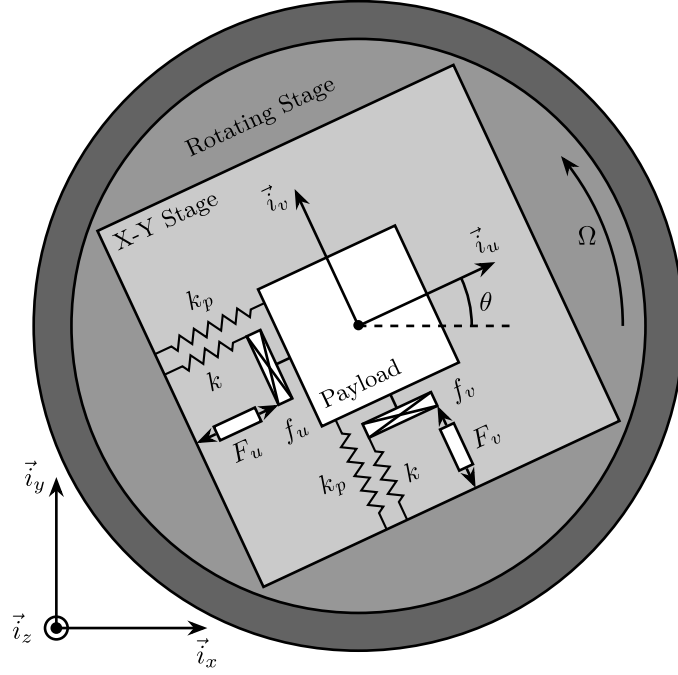
Figure 11: System with added springs in parallel with the actuators

The overall stiffness k stays constant:

$$k = k_a + k_p \tag{19}$$

$$\begin{bmatrix} f_u \\ f_v \end{bmatrix} = \boldsymbol{G}_k \begin{bmatrix} F_u \\ F_v \end{bmatrix} \tag{20}$$

$$\boldsymbol{G}_k = \begin{bmatrix} \dfrac{\left(\frac{s^2}{\omega_0{}^2} - \frac{\Omega^2}{\omega_0{}^2} + \alpha\right)\left(\frac{s^2}{\omega_0{}^2} + 2\xi\frac{s}{\omega_0} + 1 - \frac{\Omega^2}{\omega_0{}^2}\right) + \left(2\frac{\Omega}{\omega_0}\frac{s}{\omega_0}\right)^2}{\left(\frac{s^2}{\omega_0{}^2} + 2\xi\frac{s}{\omega_0} + 1 - \frac{\Omega^2}{\omega_0{}^2}\right)^2 + \left(2\frac{\Omega}{\omega_0}\frac{s}{\omega_0}\right)^2} & \dfrac{-\left(2\xi\frac{s}{\omega_0} + 1 - \alpha\right)\left(2\frac{\Omega}{\omega_0}\frac{s}{\omega_0}\right)}{\left(\frac{s^2}{\omega_0{}^2} + 2\xi\frac{s}{\omega_0} + 1 - \frac{\Omega^2}{\omega_0{}^2}\right)^2 + \left(2\frac{\Omega}{\omega_0}\frac{s}{\omega_0}\right)^2} \\[4ex] \dfrac{\left(2\xi\frac{s}{\omega_0} + 1 - \alpha\right)\left(2\frac{\Omega}{\omega_0}\frac{s}{\omega_0}\right)}{\left(\frac{s^2}{\omega_0{}^2} + 2\xi\frac{s}{\omega_0} + 1 - \frac{\Omega^2}{\omega_0{}^2}\right)^2 + \left(2\frac{\Omega}{\omega_0}\frac{s}{\omega_0}\right)^2} & \dfrac{\left(\frac{s^2}{\omega_0{}^2} - \frac{\Omega^2}{\omega_0{}^2} + \alpha\right)\left(\frac{s^2}{\omega_0{}^2} + 2\xi\frac{s}{\omega_0} + 1 - \frac{\Omega^2}{\omega_0{}^2}\right) + \left(2\frac{\Omega}{\omega_0}\frac{s}{\omega_0}\right)^2}{\left(\frac{s^2}{\omega_0{}^2} + 2\xi\frac{s}{\omega_0} + 1 - \frac{\Omega^2}{\omega_0{}^2}\right)^2 + \left(2\frac{\Omega}{\omega_0}\frac{s}{\omega_0}\right)^2} \end{bmatrix} \tag{21}$$

5.3 Effect of the Parallel Stiffness on the Plant Dynamics

$$\alpha > \frac{\Omega^2}{\omega_0{}^2}$$
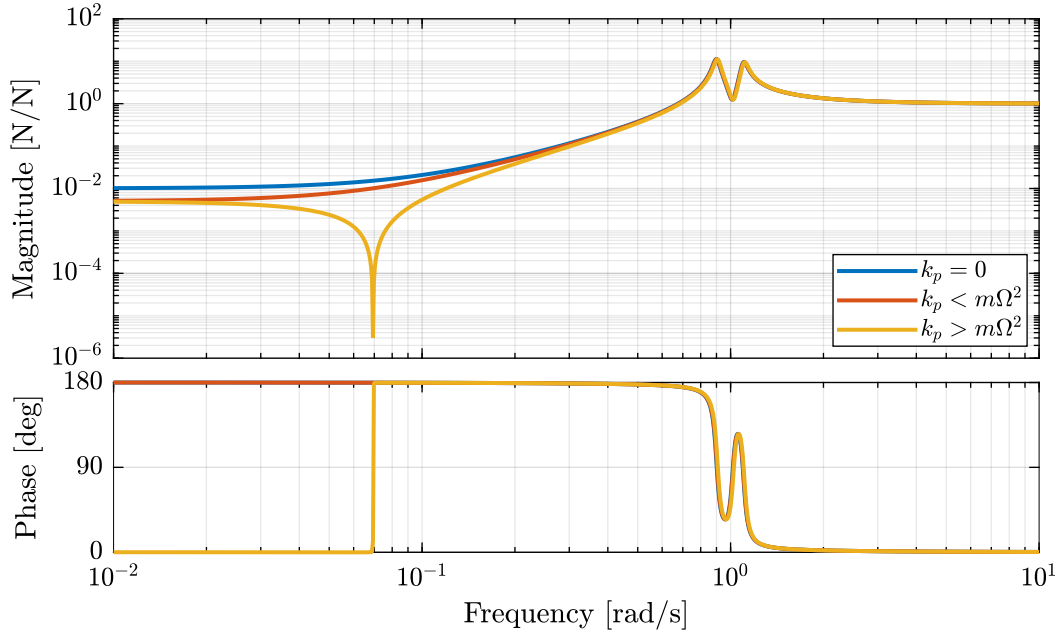$$\Leftrightarrow k_p > m\Omega^2 \tag{22}$$

Figure 12: Bode Plot of f_u/F_u without parallel spring, with parallel springs with stiffness $k_p < m\Omega^2$ and $k_p > m\Omega^2$
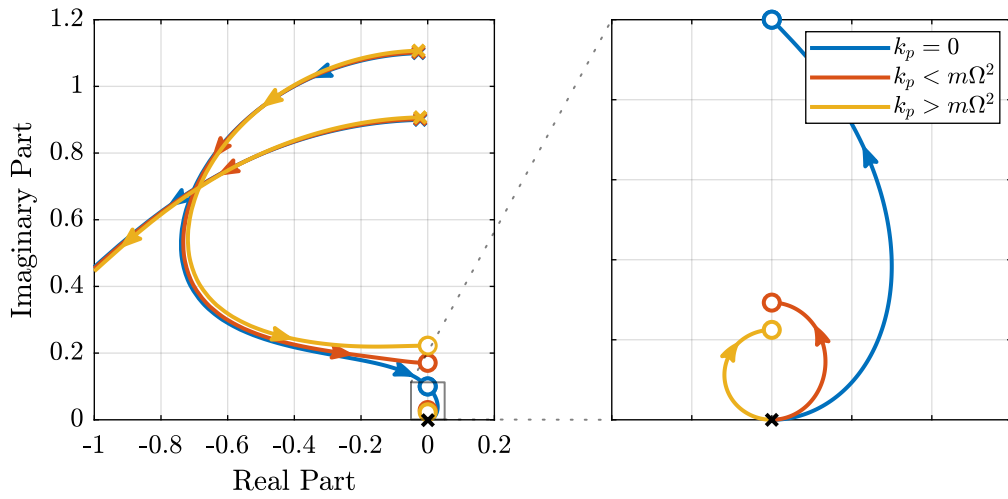

Figure 13: Root Locus for IFF without parallel spring, with parallel springs with stiffness $k_p < m\Omega^2$ and $k_p > m\Omega^2$

(a) Three values of k_p

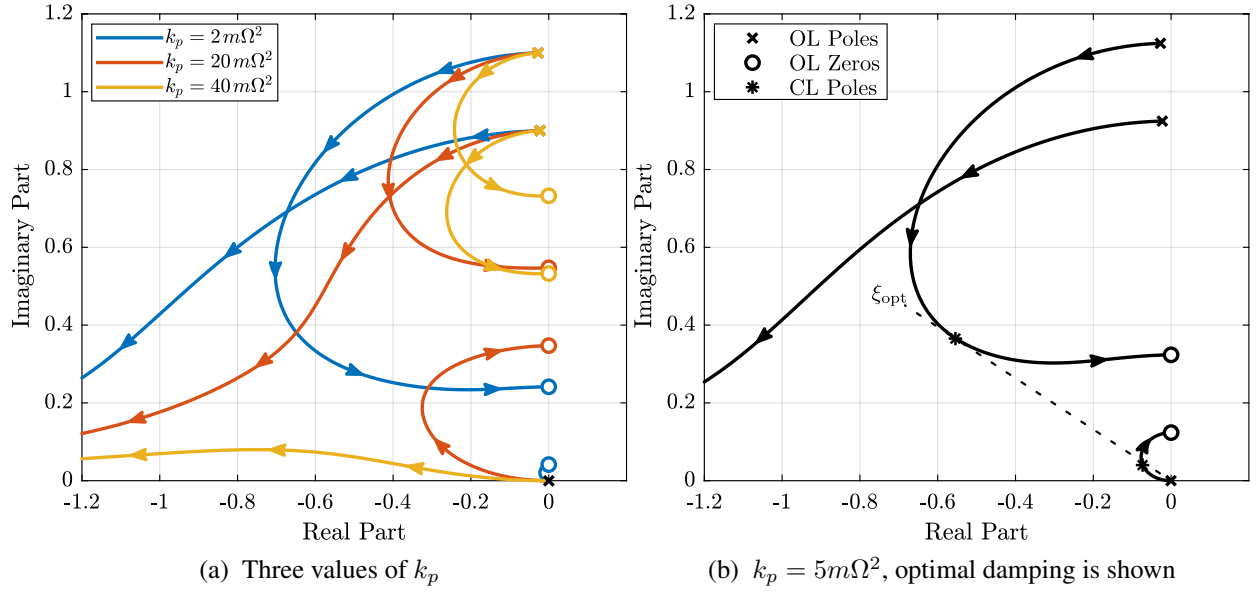(b) $k_p = 5m\Omega^2$, optimal damping is shown

Figure 14: Root Locus for IFF when parallel stiffness is used
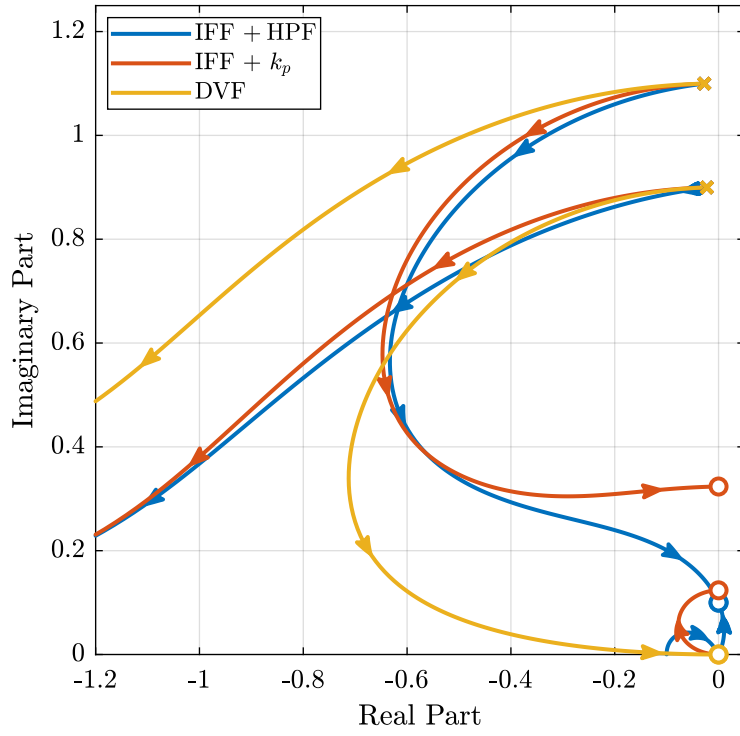

Figure 15: Root Locus for the three proposed decentralized active damping techniques: IFF with HFP, IFF with parallel springs, and relative DVF

5.4 Optimal Parallel Stiffness

6 Comparison of the Proposed Active Damping Techniques for Rotating Positioning Stages

6.1 Physical Comparison

6.2 Attainable Damping

6.3 Transmissibility and Compliance
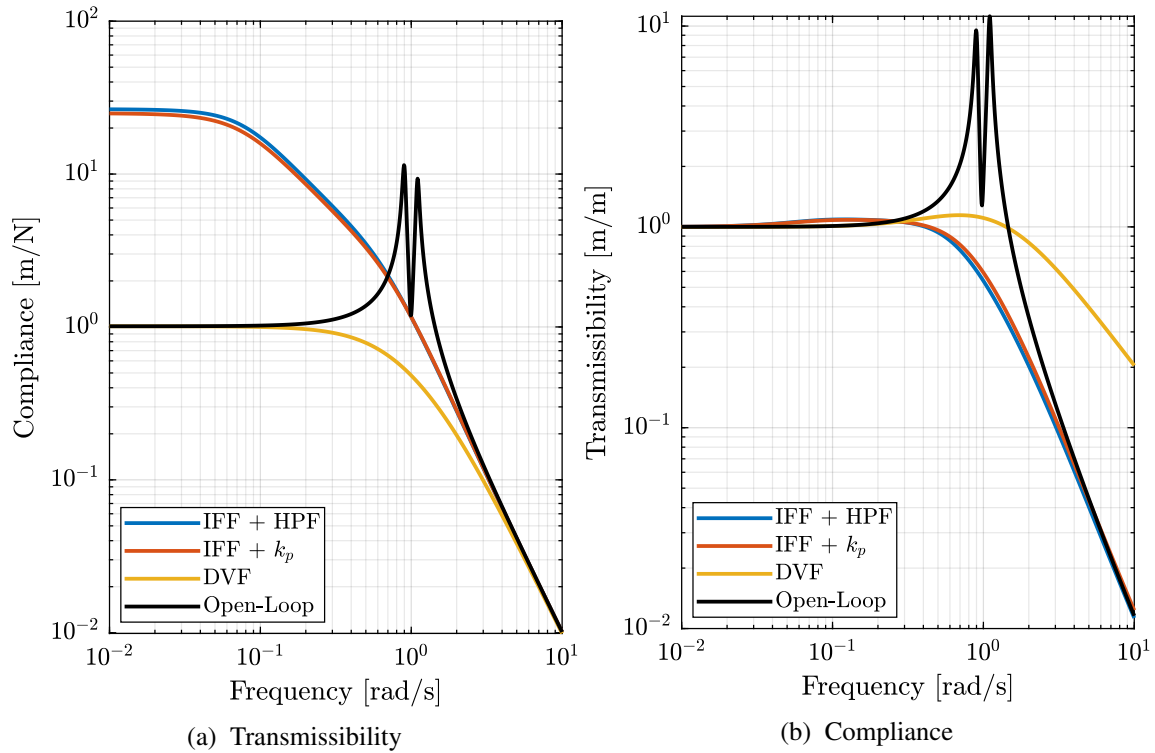

(a) Transmissibility

(b) Compliance

Figure 16: Comparison of the three proposed Active Damping Techniques

7 Conclusion

Acknowledgment

References

[1] T. Dehaeze, "Active damping of rotating positioning platforms," Source Code on Zonodo, 07 2020. [Online]. Available: https://doi.org/10.5281/zenodo.3894342